Proc Indian Natn Sci Acad **79** No. 4 December 2013 Spl. Issue, Part A, pp. 725-733
© *Printed in India*.
DOI: 10.16943/ptinsa/2013/v79i4/48008

Research Paper

Foreign Object Damage Analysis of Leading Edge of Fan Rotor Blade

RAJEEV JAIN*
SIMA (B) Department, Gas Turbine Research Establishment, C V Raman Nagar, Post Office Box : 9302, Bangalore 560 093, India

(Received 25 February 2013; Accepted 18 April 2013)

Foreign object damage (FOD) arises due to ingestion of small hard particles like small pebbles and sand particles in gas turbine engines. The damage caused due to impact of foreign object on leading edge of rotating blade results in premature crack initiation and thereafter failure of the blade due to the time-varying tensile loads in running engine. Residual stresses which arise due to impact of foreign object play an important role in controlling the rate of crack initiation and propagation. Acceleration and retardation of crack growth depends on the characteristics of stress whether it is tensile or compressive in nature ahead of the incipient crack. In the present study impact of spherical projectile against leading edge of a typical fan blade test specimen was simulated using commercially available finite element solver LS-DYNA. Deformed geometry of crater in test specimen is compared with the experimental result. Variation of residual stress in three directions along depth has been studied to predict location of crack initiation for various impact speeds. Finally, stress concentration factor has been obtained for the evaluation of fatigue life of the test specimen.

Key Words: Foreign Object Damage (FOD); Fan Blade; LS-DYNA; Fatigue Life; High Cycle Fatigue (HCF) and Low Cycle Fatigue (LCF)

1. Introduction

Foreign-Object-Damage (FOD) occurs due to ingestion of hard particles [1] while the engine is flying, taxing or running on runway with ideal speed. These events usually take place during takeoff and landing when loose debris from the airfield, with sizes in the millimeter regime on the ground gets ingested into the engine. Velocity of the ingested object varies from 100-350 m/s, depending on the engine specification as reported by Chen and Hutchinson [2]. These ingested objects cause damage and lead to reduction in strength after impacting stationary and rotating components of gas turbine engine. It is a matter of concern for both military and civilian engines due to its extremely deleterious effect on rotating components in modern aircraft engines. Life of engine components such as blades depends on large number of fatigue cycles under vibrating loads, superimposed on high mean stress.

Foreign object damaged rotor blades are subjected to high-cycle fatigue (HCF) loading from vibrations and resonant airflow dynamics. High-cycle fatigue (HCF) failures in jet engines have been attributed to a combination of high-frequency vibratory loading and prior damage from other in-service contributors such as FOD, fretting or contact fatigue, and low-cycle fatigue due to centrifugal loads [3]. Generally, engine manufacturers evaluate fatigue life of compressor blades by subjecting the components to vibratory loads. Damage produced in engine component due to foreign object is introduced at expected critical locations and thereafter tested to determine the remaining fatigue life. There is barely any reported work on the evaluation of fatigue resistance under HCF conditions due to FOD damaged components [4]. Method of inflicting real or simulated FOD is extremely important to assess real fatigue life of engine components. Real FOD can

*For Correspondence: E-mail: rajeevjain63@gmail.com

be produced by shooting typical objects ingested into an engine at velocities and incident angles expected under operational conditions.

Experimental and computational work is getting enormous attention of scientists and engineers in FOD analysis. Present numerical codes have the capabilities of including non-linear stress-strain variation with strain-hardening and strain-rate dependent material effects in the high velocity impact phenomena. In most of the finite element (FE) studies, residual stresses are produced due to shot-peening process. Hong *et al*. [5] evaluated residual stresses in a 3-D object using FE numerical technique and studied the effect of initial yield stress, impact velocity, shot diameter and incident angle of impact.

Meguid and his co-authors [6, 7] examined the effect of shot and target parameters upon the plastic zone development and induced residual stresses using DYNA-3D FE code. Foreign object impact on rotor blades produce indentation having size in the millimeter regime with impact velocities varying from 200-350 m/s, depending on the blade speed of a specific engine [8, 9]. Although it is possible to assess residual stress, stress concentration factor and crater geometry using FE technique but it is not possible to predict fatigue life of damage component. Numerical codes have the difficulty to include degradation of material properties due to FOD. Apart from this, present codes do not have built in provision to consider FE modeling of natural crack produced due to FOD. Thus, there are very complex phenomena which are occurring simultaneously due to FOD; therefore it is difficult to evaluate fatigue strength of the component using finite element technique.

Experimental simulations of FOD can be achieved by machining a notch in the material of a size to match real FOD from field experience. Nicholas *et al*. [10] conducted series of impact experiments on leading edges of titanium test specimen and compared their results with those on machined notches. This can be done using quasi-static indentation of a chisel with an appropriate radius to the proper depth, by pendulum or drop weight impacts at various angles to the leading edge including a side impact chisel, or any other method such as a solenoid gun to produce the required geometry of notch. It has not yet been established that any of the simulation methods produce conditions identical to those of real FOD from ballistic impacts in terms of residual stress fields or material damage ahead of the notch. In fact, it has been shown recently that ballistic impacts and quasi-static chisel indents which produce nearly similar size craters in a leading edge do not produce the same HCF resistance under tensile loading [11].

Extensive research work has been done on low and high cycle notch fatigue test, but it cannot be extended to solve the problems of components damaged by foreign object, due to several prominent reasons. Evaluation of fatigue life due to FOD is a complex phenomenon as it involves understanding of impact mechanics, fracture mechanics and fatigue behavior of the material simultaneously. The damage in the region of impact often becomes the site of early crack initiation and propagation. Mall *et al*. [12] demonstrated that impact of foreign object modify micro-structure of material due to high strain deformation, give rise to stress concentration due to indentation and induce local tensile and compressive residual stress around location of impact. Assessing the influence of each factor to study fatigue behaviour of damaged component is extremely difficult. Peters and Ritchie [13] studied the effect of microstructure in titanium material due to FOD and later Peters *et al*. [14] used Kitagawa-Takahashi approach to evaluate high cycle fatigue limit of a component subjected to FOD. A similar kind of approach has been suggested by Nowell *et al*. [15, 16].

There is hardly any systematic investigation on the effect of FOD on the fatigue properties of materials. Most of the analyses focus on the reduction of fatigue life due to FOD. Foreign object impact give rise to plastic deformation that induces residual stresses near the vicinity of the indentation. Damage ahead of the ensuing indentation reduces fatigue properties of the material which cannot be quantified easily by any conventional means. Shape and size of the crater produce due to impact is complicated and cannot be defined by radius and depth. Also, impact

damage produces cracks and thus changes nature of the problem from crack initiation to propagation. It is essential to study the fracture aspects of the material and geometry for accurate prediction of crack growth.

In the present investigation, numerical analysis has been carried out to predict contact forces, maximum and residual deformation due to impact of spherical glass projectile. Foreign object damage analysis was simulated by impacting the small hardened spherical glass object of 1.0 mm diameter against leading edge of a titanium alloy test specimen blade. Size of the crater produced using spherical projectile is compared with experimental work. Residual stresses have been evaluated at normal impact for five different velocities using commercially explicit finite element solver LS-DYNA and stress concentration factor has been evaluated using implicit finite element solver ABAQUS. These values can be used to predict fatigue life of the test specimen using standard S-N curve or testing the specimen under cyclic loading in the laboratory.

2. Testing Procedure

Test sample is impacted with a glass spherical ball of 1.0 mm diameter using a single-stage compressed gas gun. Experimental set-up has a facility to launch the projectile with a maximum speed of 305 m/sec. The glass sphere was chosen as being representative, in both size and properties, of sand or runway debris that is of concern in gas turbine operational engines. It also produces damage which is geometrically similar to what is sometimes observed in the aero field.

Glass sphere is held at the center of a sabot after drilling a shallow hole greater than 1.0 mm diameter. A steel plate with an internal hole diameter smaller than the sabot diameter was secured at the end of the gun barrel to stop the sabot, yet allow the glass bead to continue in flight. The actual glass bead was in free flight for approximately 19 mm. This free flight distance permitted accurate measurement of the projectile velocity while still facilitating precise location of the impact. A telescopic bore scope was located behind the gun and used to sight the target and adjust trajectory.

2.1 Geometry

The airfoil specimen configuration is a diamond cross-section tension specimen [17], the geometry of which is shown in Fig. 1. This test specimen have been fabricated from a forged stock round bar of 45 mm diameter. The edges of the gage section are tapered to a radius representative of the leading edge of a typical fan blade of gas turbine engine. Leading edge radius of the blade is 0.38 mm the cross section of test section is shown in Fig. 1.

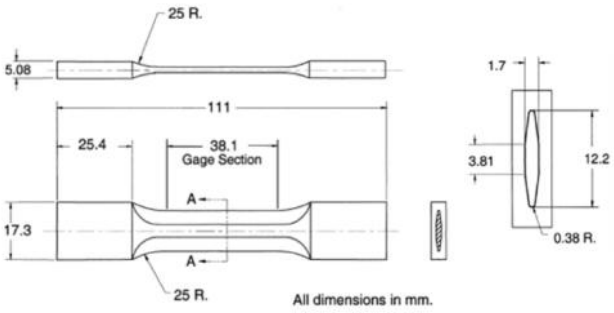

Fig. 1: Geometry of the leading edge test specimen and cross section dimension for FEM simulation [17]

2.2 Finite Element Mesh

Finite element (FE) model of test specimen similar to leading edge of fan blade shown in Fig. 1 was modelled using HYPERMESH finite element pre-processor. Present model has very fine mesh near the vicinity of the impact to achieve higher accuracy in numerical simulation during 3-D dynamic event. In order to save computer time, coarse mesh was generated slightly away from the region of impact with smooth transition from fine to coarser elements. Three dimensional FE models of both test specimen and spherical projectile were discretised using eight node brick elements as shown in Fig. 2. This figure shows the section model of spherical projectile of one mm diameter consisted of 13,600 solid brick elements and 14,939 nodes with an element size of approximately 0.02 mm at the vertex. This model is specifically shown in section view for indicating mesh portion in the vicinity of impact. The fan blade test specimen is meshed using 3,39,522 eight-node brick elements, with a graded distribution where the mesh

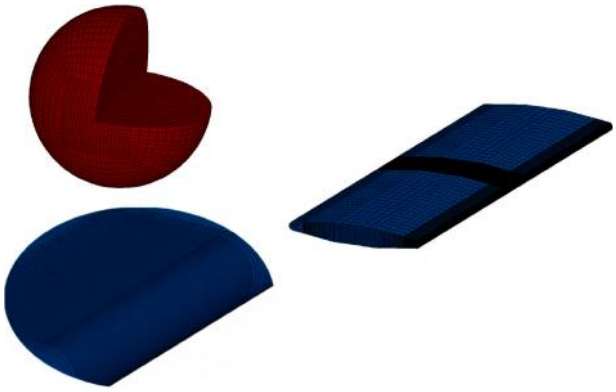

Fig. 2: Finite element model of spherical projectile and test specimen

density near the impact site is very high. Element formulation in both models is reduce integration. The smallest element, nearest to the point of impact, had a minimum element size of 0.4 mm. The time increment in the explicit analysis is the time for an elastic wave to traverse the smallest element, which is of the order of 10^{-10} second in the present analysis.

In order to reduce error during finite element simulation, several trials have been done to improve the quality of the mesh elements by re-meshing the impacting projectile and test specimen such that hour glass energy lost during numerical simulation of impact phenomena in between spherical projectile and test specimen is the minimum. Also, default parameters have been adjusted to avoid many of the difficulties associated with FE modelling of dynamic event.

2.3 Material Properties and Material Model

Material of test specimen having configuration similar to leading edge of fan blade is titanium (Ti-6Al-4V). Similar alloy is used in fan blades of gas turbine engine. This material is almost ideally plastic with very little strain hardening. Young's modulus (E) and tensile yield stress (σ_y) is about 110 GPa and 1098 MPa respectively. Density and Poisson's ratio of this material are 4420 kg/m^3 and 0.33 respectively.

In most of the metals and alloys, the yield stress increases with increase in strain rate. Materials show a large increase in flow stress at strain rate above 10^3-10^4 s^{-1} (Clifton [18]). The maximum strain rate generated from a 305 m/s FOD was found to be above this range, and therefore rate sensitivity factor have been considered for this analysis. There are several material models which can take into account the effect of strain rate e.g. Cowper-Symond, Johnson-Cook (JC) and Zerlie-Armstrong material models. For materials with negligible strain hardening, the rate dependence can be analytically expressed in the form of Cowper-Symond power law. Although there is very less strain hardening factor in present titanium material, but for accurate prediction, JC model has been taken to consider the effect of stain hardening in numerical simulation. It is a decoupled flow stress equation having strain hardening and strain rate varying components as shown in equation (1). Local heating and its effect on the flow stress have been neglected based on estimates of adiabatic temperature changes obtained from computed plastic strains Chen and Hutchinson [19]. The Coulomb friction coefficient has a minor effect on the analysis and therefore it is taken as 0.1.

$$\sigma_{eq} = (A + Bp^n)(1 + C \ln p^*) \quad (1)$$

where A, B, C and n are material constants, $\dot{p}^* = \dot{p} / p_0$ is a dimensionless strain rate, and $\dot{p}_0$ is a user defined reference strain rate. The material properties of spherical projectile and Ti-6Al-4V are shown in Table 1. Material parameters A, B, C and n of JC model have been taken as 1098, 1092, 0.93 and 0.014 respectively [20]. The material of spherical projectile is advanced ceramics ZEMAT (ACL-2090Zero expansion glass ceramic).

Table 1: Material properties of spherical projectile and test specimen

Component	Material	Density (kg/m^3)	Young's modulus (GPa)	Poisson's ratio	Yield stress (MPa)
Sphere	ACL-2090 glass ceramic	2530	90	0.24	——
Test Specimen	Ti-6Al-4V	4420	110	0.33	1098

Initial velocity of the spherical projectile for the current simulation has been varied from 200 to 305 m/sec in the interval of 25 m/sec, whereas test specimen is held rigidly at the ends in all the direction.

The explicit finite element calculation of the dynamic impact event was performed using commercially available Lagrangian finite element code LS-DYNA [18]. To achieve a reasonable steady state in the residual stresses, the calculation was continued to 1.1 μs. Stress concentration factors have been determined by applying uni-axial tension in the deformed test specimen, using implicit finite element solver ABAQUS after impact simulation, in the absence of residual stress.

3. Results and Discussion

Present numerical simulation using LS-DYNA for impact event is of the order of few micro second duration. It is possible to reproduce exactly identical features as observed during experimental impact event using explicit finite element software, if physics of the problem is defined accurately. This section compares geometry of the crater obtained experimentally for 305 m/sec projectile speed with numerically simulated deformed geometry using Scanning Electronic Microscope (SEM). Thereafter, contact force, residual deformation and strain energy stored in blade after plastic deformation is discussed for projectile speed varying from 200 to 305 m/sec in the interval of 25 m/sec.

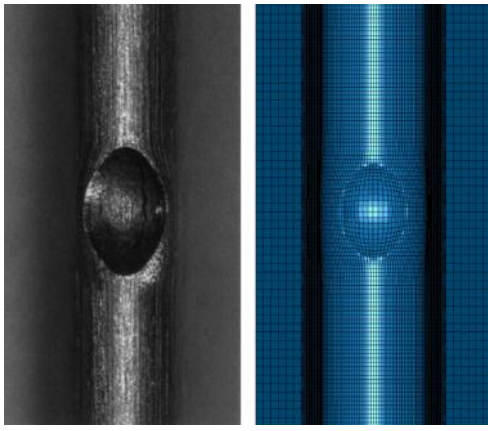

Fig. 3: Comparison of crater shape FEM analysis with test results [22]

3.1 Comparison of SEM and FEM Results

Fig. 3 shows the comparison of crater shape produce due to impact of glass ceramic projectile sphere at 305 m/sec axial velocity impacting normally on the test specimen [22] using scanning electron microscope and crater pattern obtained using finite element technique. This figure further indicates that shape and size of two figures are almost identical from every aspect and dynamic finite element analysis can be used to estimate size of the crater.

3.2 Contact Force and Deformation After Impact

Table 2 shows maximum contact force, deformation and residual deformation in the target material at different impact velocities. This table indicates that contact force, deformation and residual deformation increases with increase in impact velocity. It should be noted here that this prediction is based on the fact that material of the target component will not fail at any of the taken speed of the projectile considered in this Table.

Table 2: Variation of contact force, maximum and residual deformation with projectile velocity

Velocity (ms^{-1})	Contact force (N)	Maximum deformation (mm)	Residual deformation (mm)
200	451	0.089	0.076
225	490	0.100	0.087
250	528	0.112	0.098
275	569	0.124	0.110
305	617	0.138	0.124

Fig. 4 shows temporal variation of contact force and Fig. 5 shows variation of contact force with deformation. These figures reveal that contact force increases with increase in initial velocity of the projectile and it is the maximum at maximum penetration depth. At projectile speed of 305 m/sec this contact force is equal to 617 Newton. Maximum and residual deformation at this particular impact event is 0.138 and 0.124 mm respectively. Chen and Hutchinson [2] showed that applied static load (P)

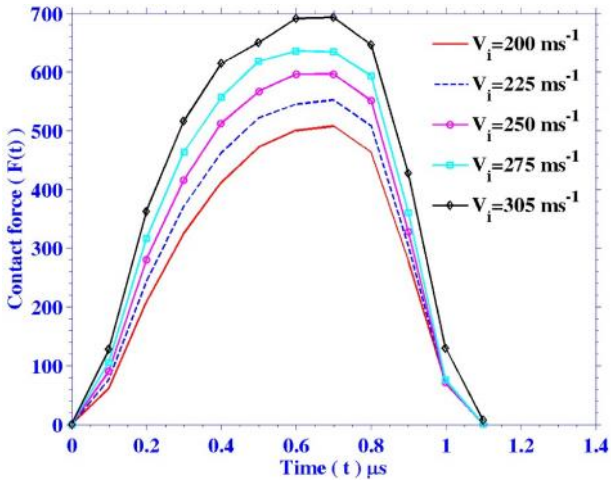

Fig. 4: Temporal variation in contact force

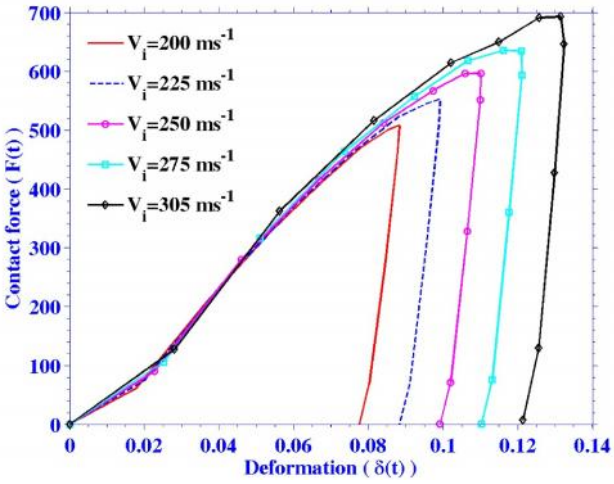

Fig. 5: Variation of contact force with deformation

varies linearly with depth (δ) and is a function of projectile diameter and yield stress of target material $P = 11.8\,\sigma_y D\delta = 2.3\,\sigma_y w^2$ for elastic perfectly plastic material property. Thus strain energy stored in the target material is $5.9\,\sigma_y D\delta^2$. For identical maximum static deformation as produced during dynamic event 1153 and 1606 Newton contact force is required.

3.3 Kinetic and Strain Energy

Kinetic energy of glass sphere of mass (m) 0.00133gms at 200 m/sec speed (v) is $0.5mv^2$ 26.4 milli-Joule. Variation of kinetic energy at speeds varying from 200 to 305 m/sec is shown in Table 3. This table also shows variation of strain energy stored during plastic deformation in blade specimen and residual kinetic energy of the projectile after impact. This table reveals that 87 to 90 percent kinetic energy of the projectile is absorbed in plastic deformation of blade material and residual rebound kinetic energy of the projectile is hardly 12 to 4.2% of total energy. Also non-dimensional parameter $KE/\sigma_y D^3$ is 0.024 for 200 m/sec projectile velocity and it increases to 0.056 for 305 m/sec projectile velocity. If it is assumed that 46% kinetic energy is lost in kinetic energy of the ricocheting particle, elastic waves in the substrate, and deformation energy in the particle then speed of the rebound particle should be 135 m/sec.

Table 3: Variation in residual kinetic energy with projectile speed

Velocity ($msec^{-1}$)	Kinetic energy (mJ)	Internal energy (mJ)	Residual KE (mJ)
200	26.40	23.19	3.18
225	33.42	29.71	3.66
250	41.24	37.03	4.15
275	49.92	45.19	4.65
305	61.50	55.60	2.60

3.4 Variation of Residual Stress along Depth

It is important to understand the variation of residual stress along depth to understand the extent up to which damage can occur. Crack prediction in a specimen can only be estimated on the basis of this variation. It is indeed an important part of the analysis to obtain residual stress after the striker impacts the leading edge. These are the stresses responsible for either growth of crack or crack arrest. Compressive stresses are mostly responsible for good fatigue life. Experimental studies on fatigue cracks near the vicinity of crater show that cracks are radial not circumferential. This is consistent with the residual stress distribution for radial stress distribution which is weakly tensile within the indent and very near to the surface.

3.4.1 Residual Stress in Depth

The normalized axial stress is shown in Fig. 6. This figure indicates that maximum tensile residual stress

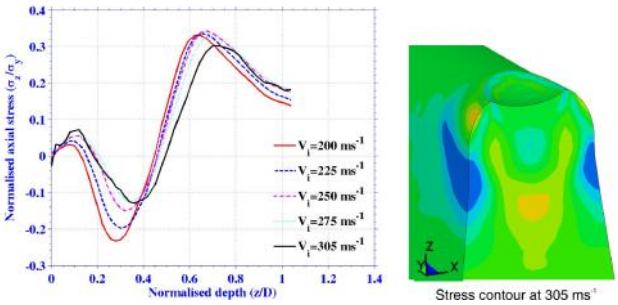

Fig. 6: Variation of residual axial stress (σ_z) at different velocities

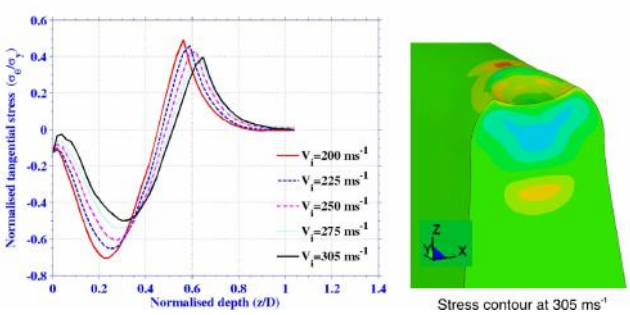

Fig. 8: Variation of residual axial stress (σ_x) at different velocities

is at a depth of 0.6 mm and its magnitude 330 MPa is the maximum at a lower speed as indicated in this figure. Stress contour at 305 m/sec projectile speed is also shown in the same figure in Z-direction.

3.4.2 Axial Residual Stress

Variation in residual stress in axial direction due to impact of spherical hard projectile is shown in Fig. 7. This figure shows that maximum tensile residual stress is at highest velocity. As an example residual stress at a depth of 0.2 mm is 744 MPa in compression and becomes tensile at a depth of 0.5 mm having magnitude of 439 MPa.

3.4.3 Radial Residual Stress

Variation in residual stress in radial direction due to impact of spherical hard projectile is shown in Fig. 8. This figure also reveals that maximum residual stress is at lowest velocity. As an example residual stress at a depth of 0.2 mm is 744 MPa in compression. Also, this stress becomes tensile after axial depth of 0.5 mm.

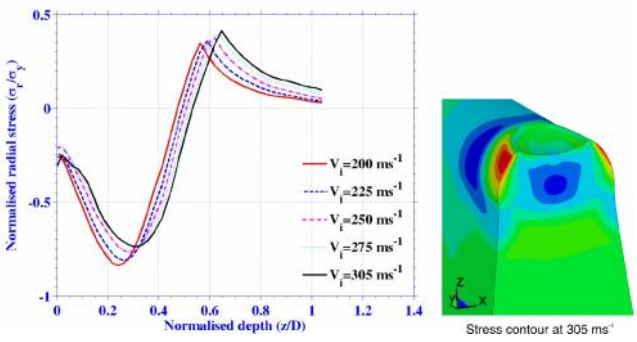

Fig. 7: Variation of residual axial stress (σ_y) at different velocities

3.5 Stress Concentration Factor

Fan blades are subjected to centrifugal load and any damage caused due to foreign object damage will initiate stress concentration factor. Stress concentration factor at various locations has been evaluated numerically using available commercial implicit finite element software ABAQUS. Three most critical regions have been considered for investigation, these are crater base marked, bulge tip marked ① ② ③ and rim marked as shown in Fig. 9 in Table 4.

Stress concentration factor at different projectile speeds is shown in Table 4. This table indicates that the stress concentration factor appears to be more significant at the bottom and rim of the crater whereas it is lesser than one at the rim location as shown in Fig. 9. This is in consistent with the fatigue crack location observed in the experiments shown by Hamrick [11] and Mall *et al*. [12]. Analysis further reveals that stress concentration factor increases with increase in projectile speed near base and rim regions. Stress contours at different projectile speeds for axial load is shown in Fig. 9. Entirely, opposite trend is found near bulge tip. The stress concentration factor at a specific location is a function of diameter of the spherical projectile D depth of penetration d plate thickness, h, and the maximum bulge width b.

3.6 Variation of Stress Concentration Factor Kt

Stress concentration factor at three identified areas i.e. crater base, bulge tip and rim have been shown with velocities varying from 200 to 305 m/sec in Fig. 10. This figure indicates that stress concentration

Table 4: Stress concentration factor at three identified locations

Velocity (m/sec)	Stress concentration factor (K_t)		
	Crater base (1)	Bulge tip (2)	Rim (3)
200	1.490	0.442	1.248
225	1.522	0.386	1.281
250	1.552	0.365	1.248
275	1.580	0.343	1.283
305	1.618	0.266	1.301

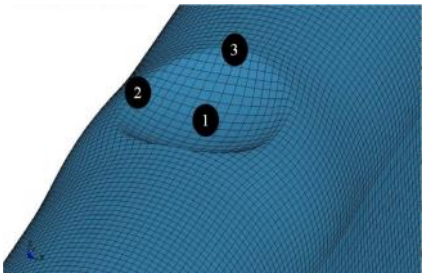

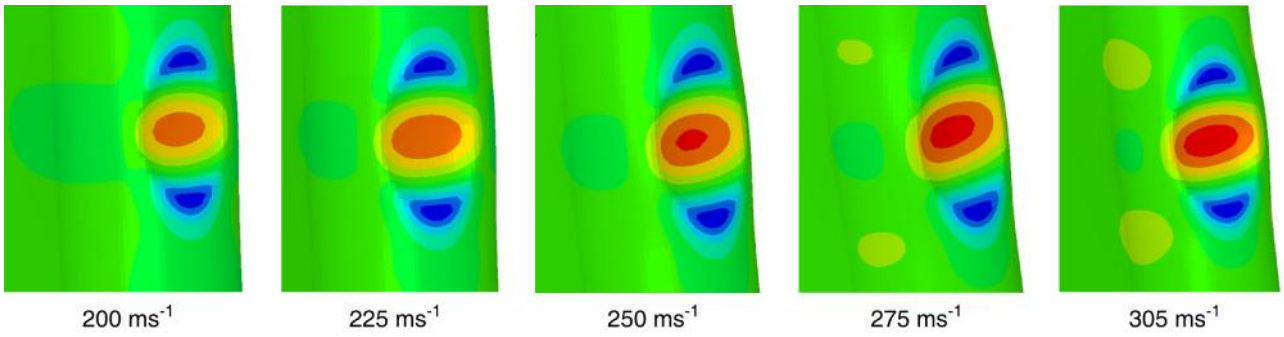

Fig. 9: Stress contour at different projectile speeds for axial load in FOD test specimen

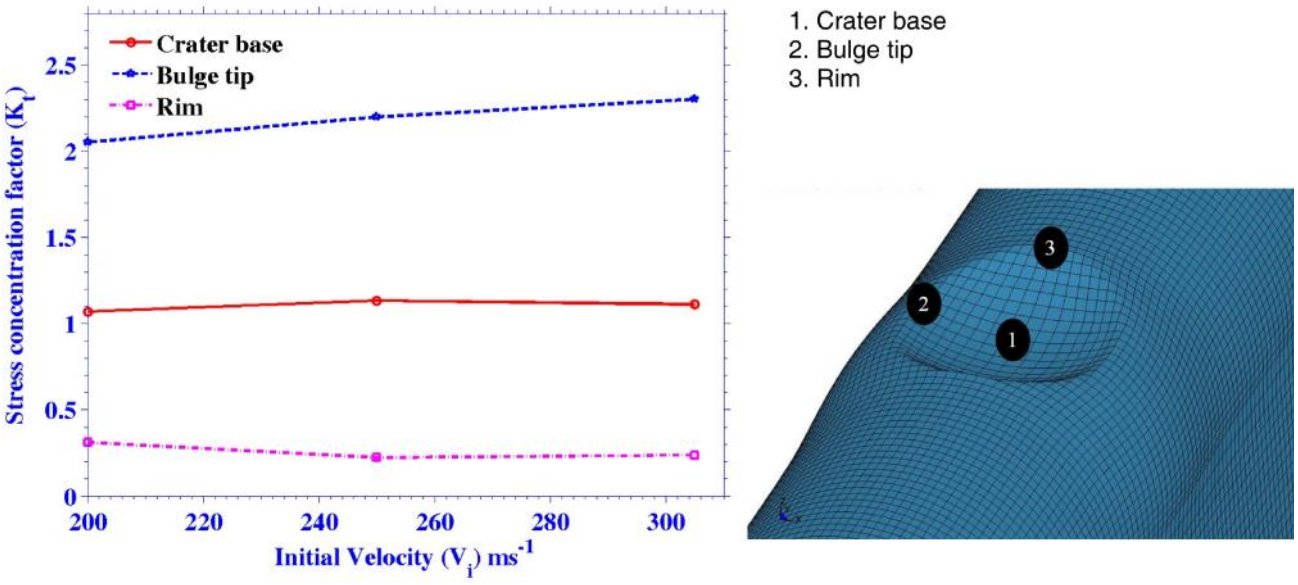

Fig. 10: Variation of stress-concentration factor with velocity

factor increases with increase in velocity of projectile at crater base and bulge tip whereas opposite trend is observed at the rim location. This figure further reveals that there is no larger variation in stress concentration factor from 200 to 305 m/sec projectile velocity considered in this investigation.

4. Conclusions

Evaluation of residual stress due to impact of foreign object is fundamental requirement for the structural integrity of engine components. Residual stress distribution is important to determine the origin of fatigue crack initiation whereas magnitude of residual stress and shape of deformed geometry is important to determine the fatigue limit. The finite element method is used to study the dynamic impact process of a rigid sphere on the leading edge of test specimen. The purpose of the present study is to address the problem of reliable stress evaluation for FOD simulation on a blade like test specimen. Explicit finite element technique has been used to determine size of the crater and residual stress and stress concentration factor in test specimen for five different velocities using simplified Johnson-Cook material model of LS-DYNA. Numerical simulation reveals that size of the crater is comparable with that of experimental test. Analysis further envisages that contact force increases with impact velocities considered in present investigation. Residual stress varies with depth, and is maximum at a distance of 0.2-0.3 mm from point of impact in all the three directions considered in the present study. Also, stress concentration factor at crater base and bulge tip increases with increase in impact velocity.

Acknowledgement

The author is grateful to the Director, Gas Turbine Research Establishment for the permission granted to publish this article in the *Proceedings of Indian National Science Academy*, New Delhi.

References

1. Nicholas T and Maxwell D C *Mechanical Behaviour of Materials* **3** (1999) 1161
2. Chen Xi and W John Hutchinson *InterJ Fracture* **107** (2001) 31
3. Nicholas T *Inter J Fatigue* 21 (1999) 221
4. Peters JO, Roder O, Boyce BL, Thomson AW and Ritchie RO *Metallurgical and Materials Transactions A* **31** (2000) 1571
5. Hong T, Ooi JY and Shaw BA *Advances in Engineering Software* **39** (2008) 743
6. Meguid SA, Shagal G, Stranart JC and Daly J *Finite Elements Analysis and Design* **31** (1999) 179
7. Meguid SA, Shagal G and Stranart JC *Material Processing* **92** (1999) 401
8. Ritchie RO, Boyce BL, Campbell JP, Roder O and Thomps *Int J Fatigue* **21** (1999) 653
9. Ritchie RO, Davidson DL, Boyce BL, Campbell JP and Roder O **22** (1999) 621
10. Nicholas T, Barber JP and Bertke RS *Exp Mech* **20** (1980) 357
11. Hamrick JL *Air Force Institute of Technology* 1999
12. Mall S, Hamrick II JL and Nicholas T *Mech Mater* **33** (2001) 679
13. Peters JO and Ritchie RO *Int J Fatigue* **23** (2001) 413
14. Peters JO *et al*. *Eng Fract Mech* **69** (2002) 1425
15. Nowell D, Dini D and Duo P *J Strain Analysis* **38** (2003) 1
16. Nowell D, Duo P and Stewart IF *Int J Fatigue* **25** (2003) 963
17. Ruschau John, Steven R and Thompson Ted Nicholas *Inter J Fatigue* **25** (2003) 955
18. Clifton RJ *J Applied Mechanics* **50** (1983) 941
19. Chen X and Hutchinson JW *J Mechanics and Physics of Solids* **50** (2002) 2669
20. Donald R Lesuer *Office of Aviation Research* Washington D. C. 20591, 2000
21. LS-DYNA Version 950 *Users Manual*, Livermore Software Technology Corporation, 1997
22. John Ruschau J, Theodore Nicholas and Steven R *Inter J Impact Engng* **25** (2001) 233.